Indonesian Journal of Science & Technology

Journal homepage: http://ejournal.upi.edu/index.php/ijost/

Simultaneous Decolorization of Tartrazine and Production of H_2 in a Combined Electrocoagulation and Photocatalytic Processes using CuO-TiO_2 Nanotube Arrays: Literature Review and Experiment

S. Slamet[1], Laily Fitri Pelawi[1], Muhammad Ibadurrohman[1], Rike Yudianti[2], Ratnawati[3,]*

[1]Department of Chemical Engineering, Faculty of Engineering, Universitas Indonesia, Depok 16424, Indonesia
[2]Research Center for Advanced Material, National Research and Innovation Agency (BRIN), Puspiptek, Serpong, Tangerang Selatan 15134
[3]Department of Chemical Engineering, Institut Teknologi Indonesia, Tangerang Selatan 15320, Indonesia
* Corresponding author, email: rnwt63@yahoo.co.id

ABSTRACTS

We reported the simultaneous decolorization of tartrazine and H_2 production via electrocoagulation and photocatalysis using CuO-doped TiO_2 nanotube arrays (TNTA) composites. Tartrazine was removed by the combination of adsorption, electrocoagulation, and photocatalytic degradation, while H_2 was produced through water reduction at the cathode and water splitting process on the photocatalyst surface. The photoreactor contains CuO-TNTA as a photocatalyst and is equipped with an 80-W UV lamp. Deposition of CuO on TNTA was conducted using a successive ionic layer adsorption and reaction (SILAR) method. The nanotubular of the TNTA as well as the distribution of CuO were evaluated employing FESEM and HRTEM. XRD patterns confirmed weak diffraction of CuO and TNTA revealing an anatase crystallite phase. The band gap of the CuO-TNTA was also found to be redshifted from that of pure TNTA. The simultaneous processes with the combined systems (20 V, pH = 11) managed to remove 80% of tartrazine while producing a high H_2 yield (1.84 mmol), significantly higher than those obtained by each process.

ARTICLE INFO

Article History:
Received 20 Aug 2022
Revised 24 Sep 2022
Accepted 09 Oct 2022
Available online 11 Oct 2022

Keyword:
CuO-TiO2 nanotube arrays,
Electrocoagulation,
Photocatalysis,
Tartrazine.

1. INTRODUCTION

The textile and food industries use organic dyes in their manufacturing processes which have become major environmental and health problems due to the toxicity and carcinogenic nature of the dyes (Soufia *et al*., 2022). Dyes are organic pollutants that have triggered many concerns because they are difficult to remove from wastewater streams (Popli & Patel, 2015). For example, is tartrazine ($C_{16}H_9N_4Na_3O_9S_2$) or acid yellow 23, which is a harmful azo and anionic dye commonly used for food coloring, pharmaceuticals, plastics, fibers, and paper (Vaiano *et al*., 2016; Okoniewska, 2021). Long-term consumption of foods containing tartrazine will potentially cause cancer, asthma, diarrhea, and hyperactivity in children that may interrupt their cognitive development (Vaiano *et al*., 2016; Amin & Al-Shehri, 2018). Therefore, it is imperative to find ways through which tartrazine is eliminated to an acceptable level using affordable and appropriate technology. According to Regulation of the National Agency of Drug and Food Control (BPOM) No. 37, the concentration of tartrazine must be reduced to at least 7.5 mg/L before it is safely disposed of to the environment.

Achieving the mentioned goals is by no means a trivial task, as many techniques have been studied without definitive success. Biological treatments are ineffective in removing tartrazine since the dye is non-biodegradable (Vaiano *et al*., 2016). The adsorption method is often deemed inappropriate because it only captures the pollutant without converting it to harmless entities (Gupta *et al*., 2011). Physical and chemical treatments have also been implemented, however, problems related to sludge formation during the process create new problems because it harms the environment (Gupta *et al*., 2011). Moreover, dye is a substance that is difficult be oxidized due to its large molecule size and complex structure. Several other techniques to eliminate tartrazine have also been conducted such as ion exchange, membrane separation, adsorption, catalytic degradation (Russo *et al*., 2021; Soufia *et al*., 2022), and various advanced oxidation processes/AOPs, such as UV/H_2O_2 (Scott *et al*., 2017). Many dye wastes can be degraded by the AOPs which use strong oxidants like ozone (O_3), hydrogen peroxide (H_2O_2), irradiation (UV/solar light), catalysts (metal oxides), or the combination thereof (Pourgholi *et al*., 2018; Javaid & Qazi, 2019). Catalytic oxidation of dyes requires active hydroxyl radicals that can be generated from, for instance, a Fenton process using iron or non-iron metal catalysts (Javaid & Qazi, 2019). However, the challenges in realizing an effective method still stand, and further developments are inevitable to design more cost-effective alternatives.

One of the most promising alternatives is electrocoagulation, which is simple, rapid, cost-effective, and easy to operate. Electrocoagulation is capable of effectively eliminating tartrazine from wastewater by coagulating the colloidal waste (Pelawi *et al*., 2019), while also producing H_2 gas which is a highly desired clean fuel (Ratnawati *et al*., 2014). However, the electrocoagulation system still has some drawbacks in terms of limited adsorption capacity, although it is still widely used for the degradation of dyes (Anantha Singh & Ramesh *et al*., 2013; Amri *et al*., 2020). Therefore, the formed coagulant still needs to be processed to avoid environmental problems. It is also important to note that it requires periodical replacements of the anodes because they are dissolved in the solution due to oxidation (Hashim *et al*., 2020).

One promising strategy to solve the mentioned problem is by combining the process with photocatalysis which can degrade pollutants chemically and, at the same time, produce H_2. Indeed, the utilization of solar energy in photocatalytic reactions has been studied extensively in the last decade, especially with a focus on its

DOI: http://dx.doi.org/10.xxxxx/ijost.vXiX
p- ISSN 2528-1410 e- ISSN 2527-8045

ability to degrade organic wastes such as tartrazine (Gupta *et al*., 2011; Vaiano *et al*., 2016; Aoudjit *et al*., 2020), and simultaneous production of renewable energy like H_2 from water or sacrificial agents (pollutants). Many researchers have developed the simultaneous degradation of pollutants and production of hydrogen considering its reliability (Cao *et al*., 2020; Jia *et al*., 2021; Zhu *et al*., 2022). TiO_2 is the semiconductor most widely used as a photocatalyst due to its cost-effectiveness, nontoxicity, stability, and activity (Ratnawati *et al*., 2014).

Electrocoagulation and photocatalysis have been used to degrade dyes, by either performing photocatalysis first followed by electrocoagulation or vice versa managed to achieve 90% pollutant removal (Boroski *et al*., 2009; Santos *et al*., 2015; Ates *et al*., 2017; Dindas *et al*., 2020). Unfortunately, the combination of the two processes is rather rare and yet to be studied intensively. To our knowledge, there is no report in the literature on the simultaneous decolorization of wastewater and H_2 production from tartrazine conducted in one integrated reactor. In such a system, the dye is adsorbed by the coagulant formed in the electrocoagulation system and degraded by the photo generated OH• radicals. At the same time, H_2 is produced by the electro-reduction of H^+ in the cathode and photocatalytic reduction on the surface of the photocatalyst. The simultaneous process between electrocoagulation and photocatalysis proposed in this study is expected to provide a more sustainable system as saturation of adsorbed pollutants can be avoided. Thus, the combined process has the potential of effective, sustainable, simultaneous decolorization of tartrazine production of hydrogen. In our previous study, we applied the same strategy for other pollutants with encouraging results (Sharfan *et al*., 2018). We also performed the combined process in a simple reactor using TNTA as the photocatalyst and coagulation at a low voltage of 5, 10, and 15 Volt (Slamet & Kurniawan, 2018), and CuO-TNTA hybrid material at specific loading of 0.06 M at pH (11), and 20 V (Pelawi *et al*., 2019).

In the present work, we investigate the combination of electrocoagulation and photocatalytic system in an integrated photoreactor for the degradation of tartrazine and generation of H_2 in different pH values and at different applied voltages. We also look at the effects of CuO loading in CuO-TiO_2 composites on the device performance. The samples were characterized using SEM, EDX, TEM, UV-Vis DRS, and XRD, the results of which are used to examine the effects of the important parameters on tartrazine removal and hydrogen production.

2. LITERATURE REVIEW

2.1. Electrocoagulation

The electrocoagulation process, a combination of coagulation, flotation, and electrochemistry, is the coagulation of colloidal particles (pollutants) in water or wastewater in the application of electric current generated from direct current (DC) power (Syaichurrozi *et al*., 2021). This method is widely used to treat wastes originating from a wide range of industries such as food (Byoud *et al*., 2017), dyes (Anantha Singh, & Ramesh, 2013), and distillery spent wash (Syaichurrozi *et al*., 2021). The process consists of three steps, namely electrolysis, coagulation, and flotation (Hashim *et al*., 2020). During these processes, Al, or Fe dissolves in the anode to form Al^{3+} and Fe^{2+} allowing electric current to flow while water is reduced in the cathode to generate H_2 and OH^- ions. Al or Fe reacts with OH^- ion to form *in situ* Al $(OH)_3$ or Fe $(OH)_2$ coagulants that can adsorb pollutants while H_2 is produced through water electrolysis. In this case, H_2 helps to float the flocculated pollutants on the surface of wastewater to generate scum (Syaichurrozi *et al*., 2021). The fact that this process also produces H_2 opens another opportunity in finding an alternative to the green production of clean fuel. With

DOI: http://dx.doi.org/10.xxxxx/ijost.vXiX
p- ISSN 2528-1410 e- ISSN 2527-8045

industrial development, the need for H_2 as renewable energy is very crucial to replace fossil fuels. Therefore, this approach can potentially synthesize an integrated system that simultaneously eliminates pollutants and generate H_2.

The reactions that occur in the electrocoagulation are as follows:

Anode: Al (s) → Al^{3+} (aq) + 3e- (1)

Cathode: $2H_2O$ (aq) + 2e- → $2OH^-$ (aq) + H_2 (g) (2)

Al^{3+} (aq) + $3OH^-$ (aq) → Al$(OH)_3$(s) (3)

Al$(OH)_3$ (s)+ pollutant → (Pollutant-Al(OH)$_3$) (s) (4)

2.2. Photocatalysis

Photocatalysis, a combination of photochemical and catalytic processes, is a chemical transformation process that utilizes photon energy from light to activate the semiconductor (Muttaqin *et al.*, 2022). The irradiation of semiconductor TiO_2 with photons (*hv*) at energy equal to or greater than its bandgap can excite the electrons in the valence band (VB) to the conduction band (CB), thereby, leaving positively charged holes (h^+) in the VB. Three possibilities will occur in the electron and hole pairs, namely: (a) some pairs recombine in TiO_2 particles (volume/bulk recombination), (b) some pairs recombine on the TiO_2 surface (surface recombination), and (c) a small number of pairs can react with donor (D) and acceptor (A) species adsorbed on the particle surface. If the electrons and holes reach the surface of the photocatalyst, they later react with water and pollutants as follows:

TiO_2 + $2hv$ → $2h^+$ + $2e^-$ (5)

H_2O + h^+ → $OH\bullet$ + H^+ (6)

$OH\bullet$ + d*ye (pollutant)* → CO_2 + H_2O (7)

$2H^+$ + $2e^-$ → H_2 (g) (8)

TiO_2 has many applications such as photocatalyst in pollutant degradation, H_2 generation from various biomass, dye-sensitized solar cells, and water splitting (Ratnawati *et al.*, 2014). In pollutant degradation, several factors affect process efficiencies such as pollutant concentration, solar intensity, the amount of photocatalyst (Nandiyanto *et al.*, 2016), and crystallite size (Nandiyanto *et al.*, 2020). TiO_2 can also be used as raw material for carbon coated Ti_4O_7 nanoparticles for electrocatalyst support (Kartikowati *et al.*, 2021). However, the use of TiO_2 still holds some downsides in terms of electron-hole recombination, inactivity under visible light illumination due to a large band gap (3.2 eV), and limited surface area. These limitations could potentially disrupt the photocatalytic performance in its applications. Therefore, some modifications have been sought, which include morphological engineering to form TiO_2 nanotube arrays, non-metal (e.g. C, N, F, or B) (Ratnawati *et al.*, 2014) and noble metal (e.g. Pt, Pd, Au, or Fe) doping (Slamet *et al.*, 2017; Muttaqin *et al.*, 2022), deposition of transition metal oxide CuO on TiO_2 (Sang *et al.*, 2019; Elysabeth *et al.*, 2021), and sensitization with WO_3, CdS, CdSe, or PbS to reduce recombination and improve the capability of harnessing visible light (Elangovan *et al.*, 2021).

TiO_2 nanotube arrays (TNTA) are usually synthesized via an anodization process in an electrolyte containing fluoride ions. Such materials are preferred due to their ability to generate large surface area while the electrolyte solution for the anodization can also contain a precursor to the non-metal dopant which can reduce the bandgap energy of TiO_2 (Ratnawati *et al.*, 2014). Moreover, CuO has also been deposited on TNTA via a successive ionic layer adsorption reaction (SILAR) method to reduce the electron-hole recombination and narrow the bandgap based on the fact that this technique exhibits better performance when compared to others as previously reported (Elysabeth *et al.*, 2021). CuO is an inexpensive and environmentally friendly material that can trap the photogenerated electrons to efficiently suppress electron-hole

DOI: http://dx.doi.org/10.xxxxx/ijost.vXiX
p- ISSN 2528-1410 e- ISSN 2527-8045

recombination (Momeni, 2015: Zangeneh *et al*., 2020). Furthermore, its narrow band gap (1.7 eV) also indicates its ability to act as a sensitizer for visible light illumination (Sun *et al*., 2013; Momeni *et al*., 2015; Zangeneh *et al*., 2020). As mentioned previously, some researchers have performed waste treatment using a combination of electrocoagulation and photocatalysis sequentially or simultaneously in one integrated reactor which can be presented in **Table 1**. Although the treatment process is similar, the conditions and variations of the process are different.

3. METHOD

3.1. Materials

Tartrazine dye ($C_{16}H_9N_4Na_3O_9S_2$), glycerol, sodium hydroxide (NaOH), ammonium fluoride (NH_4F), nitric acid (HNO_3), hydrochloric acid (HCl), and copper (II) nitrate trihydrate (Merck, PA) were purchased from Merck and used without further purification. All solutions were prepared using high purity distilled water. Thin Ti foils with a thickness of 0.025 mm were used as a base on which TiO_2 nanotube arrays are grown, while aluminium plates with a thickness of 0.05 mm, and stainless steel 316 (SS-316) with a thickness of 1 mm were used as the anode and cathode, respectively.

3.2. Synthesis of TNTA and CuO-TNTA

The Ti foil with the size of 8 cm x 2.5 cm was cleaned and washed with DI water before chemically polished using a mixture of HF, HNO_3, and water with a volume ratio of 1:3:46 to remove any impurities. TNTA was obtained via an anodization method in a cell containing an electrolyte comprising 160-mL glycerol solution, 0.5 w% NH_4F, and 25 v/v% DI water. The solution was continuously stirred for at least 10 mins. In this setup, a 2-mm-thick Pt plate with a size of 3 cm × 1.5 cm was employed as a cathode. A constant 50-V potential difference was applied using a DC power supply (Escord 6030SD) for 2-h anodization carried out at room temperature.

The CuO-TNTA was obtained by depositing CuO on TiO_2 nanotube arrays through the successive ionic layer adsorption and reaction (SILAR) method. Firstly, the TNTA was immersed in a $Cu(NO_3)_2$ solution with various concentrations of 0.04 M, 0.05 M, and 0.06 M at 75°C for 10 mins. The plate was then transferred to DI water for 30 s before being dried at room temperature for 30 s. These processes constitute one SILAR cycle. The deposition of CuO to TNTA was performed for 20 SILAR cycles. All samples were then annealed at 500°C for 3 h under atmospheric ambiance.

Table 1. Waste treatment using a combination of electrocoagulation and photocatalysis

Pollutants type	Treatment processes	Researchers
Olive washing wastewater	Photocatalysis followed by electrocoagulation or vice versa	Ates *et al*., 2017
Pharmaceutical and cosmetic wastewater	Photocatalysis followed by electrocoagulation or vice versa	Boroski *et al*, 2009
Pharmaceutical wastewater	Combination of electrocoagulation, electro-fenton and photocatalytic	Dindas *et al*, 2020
Dye	Electrochemical process and heterogeneous photocatalysis	Santos *et al*., 2015
Batik industry waste	Combination of electrocoagulation and photocatalysis	Safran *et al*., 2018
Tartrazine	Combination of photocatalysis-electrocoagulation	Slamet and Kurniawan, 2018; Pelawi *et al*., 2019
Ciprofloxacin and methylene blue	Combination of photocatalysis-electrocoagulation	Muttaqin *et al*., 2022

DOI: http://dx.doi.org/10.xxxxx/ijost.vXiX
p- ISSN 2528-1410 e- ISSN 2527-8045

3.3. Characterizations

The morphology of the synthesized TNTA and CuO-TNTA samples was examined by a scanning electron microscope (SEM, JSM-IT300 InTouchScope™ 15 kV and 7 mA) equipped with energy dispersive X-ray (EDX) spectroscopy to characterize the elemental composition. Nanostructural features of the samples were also probed using a transmission electron microscope (TEM, FEI Tecnai type G2-STWIN) operating at 200 kV along with further analysis of selected area electron diffraction (SAED). The crystallite properties of the samples were identified by an X-ray diffractometer (XRD) (PAN analytical Empyrean diffractometer) with a Cu anode tube (λ = 0.15406 nm) operating at 40 kV and 30 mA, scanned within the 2θ range of 20 – 65°.

Accordingly, the crystallite size was estimated from the full-width half-maximum (FWHM) of the XRD peaks using the Scherrer equation. The optical properties and the bandgap values of the samples were estimated using the Kubelka-Munk functions from the obtained UV-visible diffuse reflection spectra (UV-Vis DRS, Harrick Scientific, Agilent Cary 600 UV-Vis, DRS) in the range of 300-700 nm. Dye absorption was measured using a UV-Vis spectrophotometer (Shimadzu UV 1600, Japan) and the produced H_2 from the reaction system was detected employing gas chromatography (GC) (Shimadzu GC-8A) with a 5A Molecular Sieve (MS) column and high purity argon used as the carrier gas.

3.4. Electrocoagulation Test

Simultaneous decolorization of tartrazine and production of H_2 was performed in an acrylic reactor equipped with a power supply, Tedlar bag, Quartz tube, and Pyrex tube. A 316 stainless steel plate (thickness × length × wide = 1 × 11 × 2.5 cm) used as the cathode was placed between two aluminum plates (thickness × length × wide = 0.05 × 11 × 2.5 cm) which are assigned as anodes. The Pyrex tube mounted on the SS-316 plate was connected to the Tedlar bag as a hydrogen collector. The reactor is filled with 400 mL of 20-mg/L tartrazine solution at different pH values, i.e. 11 (alkaline) and 4 (acidic). Samples were collected every hour to be analyzed using UV-Vis spectrophotometry at the wavelength of 405 nm for the solution of pH = 11 and 427 nm for the solution of pH = 4. At the cathode side, hydrogen produced was measured using gas chromatography (GC).

3.5. Photocatalyst Performance Test in the Electrocoagulation-Photocatalytic System

The effects of combining the electrocoagulation and photocatalytic processes were evaluated by adding TNTA or CuO-TNTA to the reactor system (depicted in **Figure 1**), irradiated by UV lamps (Sankyo Denki, 80 W, 365-nm wavelength). The aluminum plates and SS-316 for electrocoagulation tests and TNTA photocatalysts were placed in an acrylic reactor connected to a Tedlar bag which was used as a gas reservoir. The reactions were conducted in 4 hours and the effects of pH (i.e. 4 and 11) and the applied voltage (i.e. 20, 30, 40, and 50 V) were studied. Meanwhile, the depletion of tartrazine concentration was monitored using a UV-Vis spectrophotometer (Shimadzu UV 1600, Japan) and calculated using the following Eq. (9):

$$\% \text{ decrease} = \frac{C_{initial} - C_{final}}{C_{initial}} \times 100\% \qquad (9)$$

where $C_{initial}$ and C_{final} are the initial and final concentrations of tartrazine, respectively.

DOI: http://dx.doi.org/10.xxxxx/ijost.vXiX
p- ISSN 2528-1410 e- ISSN 2527-8045

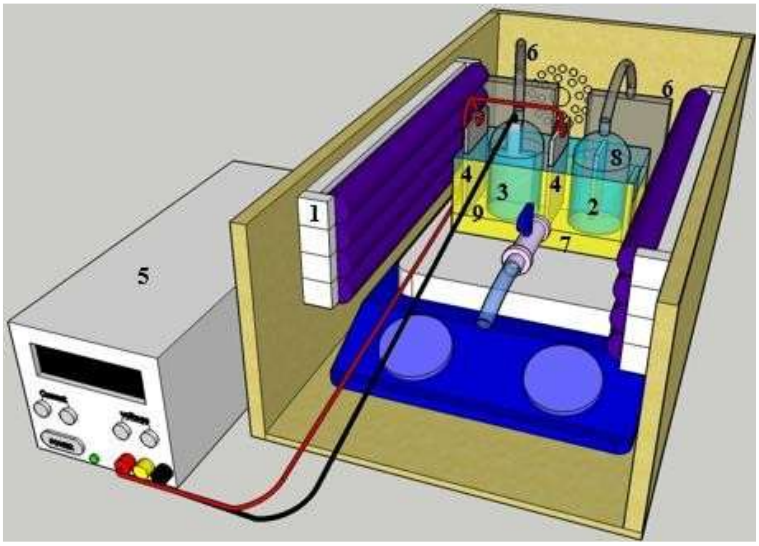

Figure 1. Reactor vessel for the combination of electrocoagulation and photocatalytic process.

The kinetics of the degradation has been described by the Langmuir-Hinshelwood kinetic model (Nandiyanto *et al*., 2020) (Eq. 10) as follows:

$$-\frac{dC}{dt} = \frac{k_T.K_C.C}{1+K_C.C} \quad (10)$$

where C is the concentration of tartrazine at a specific time t, k_T is the apparent reaction rate constant, K_C is the apparent equilibrium adsorption coefficient. When the initial reactant concentration (C_0) is low, the expression model of Eq. 10 becomes:

$$-\frac{dC}{dt} = kC^n \quad (11)$$

For first-order degradation kinetics, it can be calculated by integrating the above Eq. (11) with order n = 1, therefore Eq. (11) becomes:

$$\ln\left(\frac{C_t}{C_0}\right) = -k_1 t \quad (12)$$

where C_t is the concentration at time t, C_o is the initial concentration, and k_1 is a kinetic constant for order 1. Plotting of Eq. (12) namely ($\ln\left(\frac{C_0}{C_t}\right)$ vs t will obtain k_1 as a slope.

4. RESULTS AND DISCUSSION

4.1. Photocatalyst Characterization

Micrographs depicting the surface morphology of TNTA and CuO-TNTA composites are shown in **Figure 2**. Superficially, no significant differences were observed in the morphological structure of all four samples. However, upon further scrutiny, it was found that CuO deposition induces a slight increase in the inner diameter of the tubes as Cu concentration increases.

The wall thickness of the tubes, on the other hand, remains relatively unaffected, as presented in **Table 2**. It is well documented that water content and mechanical stirring during anodization may contribute to the eventual dimension of nanotubes (Elysabeth *et al*., 2021), while the nanotubular structure of TiO_2 is dependent on the competition between the formation of oxides on the uppermost layer of the plate and the dissolution into the electrolyte solution (Ratnawati *et al*., 2014). Upon increasing the concentration of CuO precursor ($Cu(NO_3)_2$) from 0.04 to 0.06 M, the inner diameter of the tubes increases, possibly due to the sintering effects of calcination on particle size. The concentration of precursor solution of $Cu(NO_3)_2$ might affect the mobility of CuO incorporating amorphous regions. Upon calcination, the amorphous phase is converted to a crystal phase, thereby increasing the conductivity of CuO which further causes an increase in the tube diameter.

DOI: http://dx.doi.org/10.xxxxx/ijost.vXiX
p- ISSN 2528-1410 e- ISSN 2527-8045

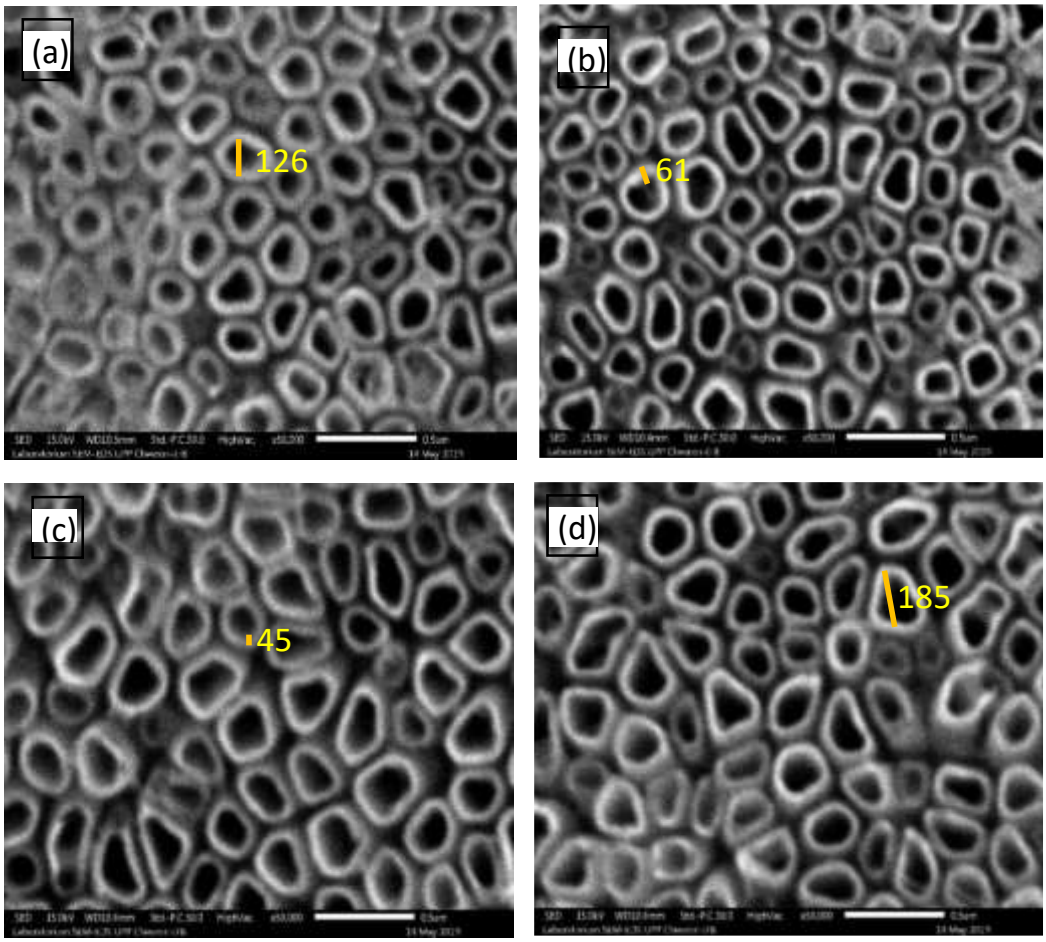

Figure 2. SEM image of (a) Amorphous TNTA, (b) 0.04 M of CuO-TNTA, (c) 0.05 M of CuO-TNTA, and (d) 0.06 M of CuO-TNTA.

Table 2. The average tube diameter, average tube wall thickness, and EDX analysis of various photocatalyst.

Photocatalyst	Average tube inner diameter (nm)	Average tube wall thickness (nm)	% Weight of Component				
			Cu	Ti	O	C	F
TNTA (amorphous)	134	47	0	53.15	28.74	17.2	0.96
0.04 M of CuO-TNTA	149	44	0.40	60.67	30.23	7.58	1.13
0.05 M of CuO-TNTA	158	50	1.09	61.25	30.06	6.47	1.40
0.06 M of CuO-TNTA	166	52	1.68	58.52	33.12	5.97	0.68

It is important to note that the amorphous TNTA comprises porous structures which become denser after annealing. The results of our previous studies also found that the tube diameter of crystallite TNTA became larger after amorphous TNTA was calcined at 500°C (Ratnawati *et al.*, 2015). CuO bonding on the TNTA surface might also change the molecular configuration, which is indicated by the increase in the inner diameter of the tube. Meanwhile, the TiO_2 nanotube arrays surface in the amorphous form was covered by the remaining glycerol electrolyte solution as indicated by rather high carbon content, resulting from the decomposition of glycerol into carbon as indicated by the EDX analysis results, shown in **Table 2**. EDX analysis also identifies flour content in the nanotubes, which is likely to be originated from NH_4F leftover (Ratnawati *et al.*, 2014). Importantly, the content of Cu in CuO-TNTA composites is found to be 0.4%wt, 1.09%wt, and 1.68%wt,

DOI: http://dx.doi.org/10.xxxxx/ijost.vXiX
p- ISSN 2528-1410 e- ISSN 2527-8045

corresponding to $Cu(NO_3)_2$ concentrations of 0.04, 0.05, and 0.06 M, respectively.

The procedures for interpreting and calculating the average tube inner diameter of TNTA (**Figure 2**) using SEM are (1) determination of the morphological shape (irregular tube) and (2) analysis of scale bar/diameter size. The second step includes identifying the scale bar on the SEM image and comparing it with the diameter size of TNTA, measuring the minimum/maximum Feret diameter according to the number of samples, calculating the average Feret diameter of each sample [(d max + d min)/2], and finally calculating the average of Feret diameter for all samples as shown in **Table 2** (Yolanda and Nandiyanto, 2022). Tube wall thickness was also calculated by measuring the thickness of each tube and then averaged according to the number of existing tubes.

The nanostructure of the composites was further probed utilizing TEM and SAED analyses, presented in **Figure 3**. From the micrograph depicted in **Figure 3a**, it is inferred that Cu was successfully deposited on TiO_2, corroborating the finding from EDX analysis. The CuO nanoparticles are distributed on the wall of the nanotubes with a thickness of 22-26.24 nm and an inner diameter of 244.9-248.9 nm. However, the average values of wall thickness and inner diameter are lower, as informed in **Table 1**. This may indicate that the closer the tubes are to their bottom part, the larger their diameter would be. The longer the anodizing time, the more $[TiF6]^{-2}$ dissolves from the inner part of the tubes, thereby increasing the inner tube diameter. This condition imposes a challenge for CuO to enter the inner side of the tubes. **Figure 3a** shows that CuO is well distributed on the outer surface of TNTA. **Figure 3b** reveals the interplanar distance d(111) at 0.22 nm that originates from the CuO crystal region, conforming to the XRD signal of CuO at 2θ of ca. 38.77°. **Figures 3b** and **3d** depict the crystal lattice of TiO_2 with a d-spacing of 0.35 nm, attributable to (101) anatase crystallite phase. To further investigate the crystal structure of the synthesized nanocomposites, SAED analysis was sought and the patterns are shown in **Figure 3c**, illustrating the calculated interplanar distances (dhkl) in the cases of CuO (111) and TNTA (101), (004), (200) and (105).

The XRD patterns of TNTA and CuO-TNTA samples are illustrated in **Figure 4** to scrutinize their crystallite properties studied using XRD as depicted in **Figure 4**. The diffraction signals emerging at 2θ of 25.52, 37.98, 48.24, and 54.08° correspond to the anatase crystallite according to the Miller indices of (101), (004), (200), and (105), respectively (JCPDS No. 21-1272) (Meng *et al*., 2016; Elysabeth *et al*., 2021), while other peaks are attributable to the metallic titanium. On the other hand, no signal of rutile phase is observed, e.g. at 27.37, 36.02, 41.16, or 56.53° with diffraction fields of (110), (101), (111), and (220) (JCPDS No. 21-1276). Interestingly, the increased amount of Cu in the composite led to the higher peak intensity of the anatase phase, indicating that the crystal formation is somewhat more effective in the case of Cu-deposited nanotubes. This may be associated with the high thermal conductivity of CuO which allows more effective heat conduction during the calcination of the samples (Ahn *et al*., 2013; Elysabeth *et al*., 2021). The crystallite size of the TNTA samples was estimated using the Debye–Scherrer equation (Elysabeth *et al*., 2021), revealing values in the range of 26.9 – 28.5 nm, as inferred from Table 3. A weak diffraction peak is detected at 2θ of ca. 38.77° assigned to the (111) plane of CuO crystal according to JCPDS 8012 68 (Raul *et al*., 2014). This phenomenon agrees with EDX results, in which the low amount of Cu element was confirmed. Moreover, the low Cu concentrations also provide an advantage since they did not lead to a shading effect thereby, not reducing the active site of the TiO_2 nanotube arrays photocatalyst (Janczarek & Kowalska,2017).

DOI: http://dx.doi.org/10.xxxxx/ijost.vXiX
p- ISSN 2528-1410 e- ISSN 2527-8045

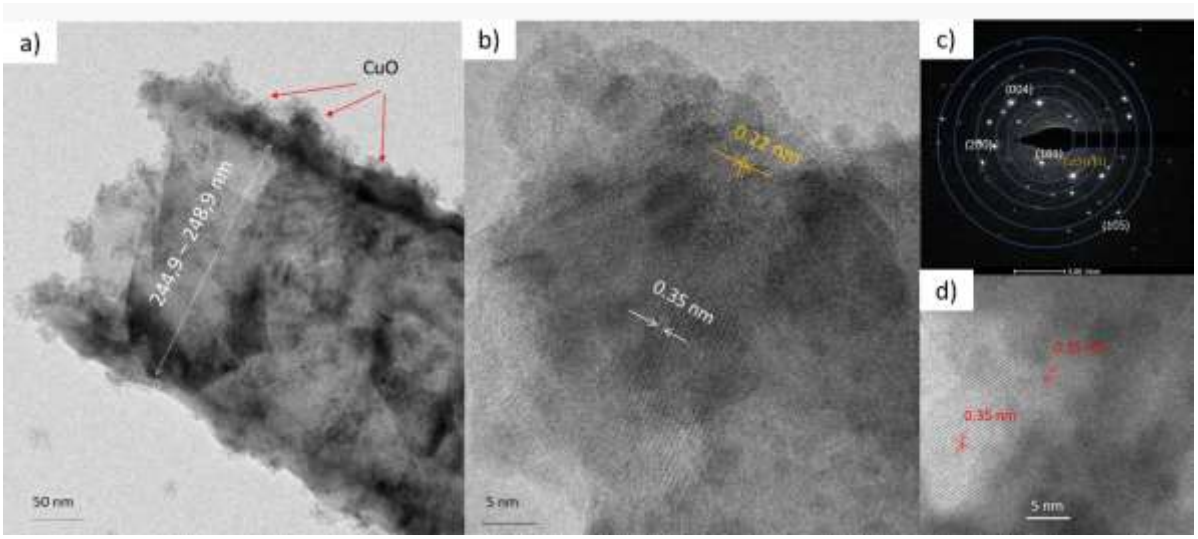

Figure 3. TEM image a) CuO distribution, b) and d) lattice structure, c) SAED patterns of TNTA-CuO Hybrid Structure.

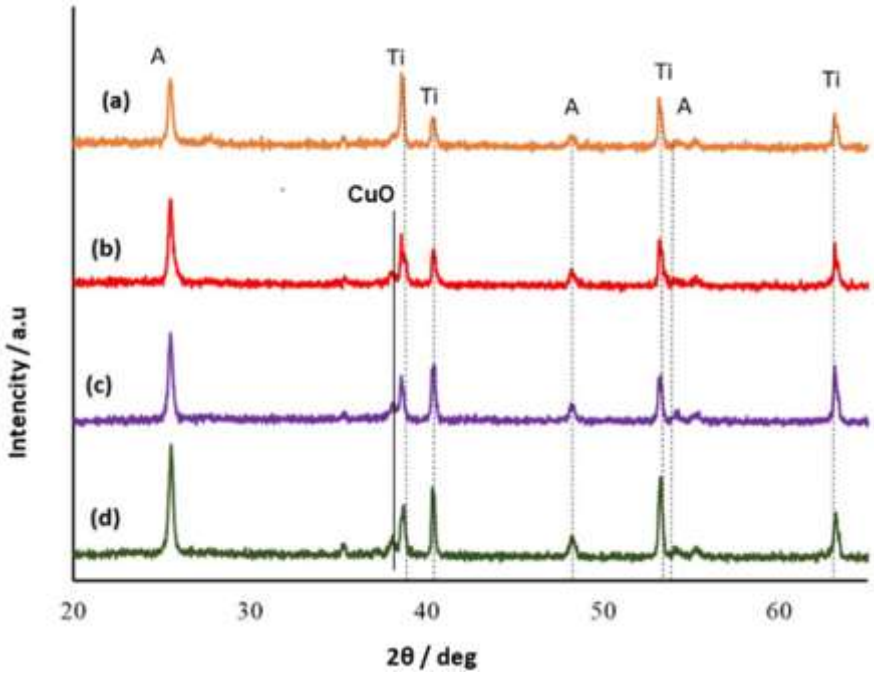

Figure 4. XRD patterns of various photocatalysts samples (a) TiO_2 nanotube arrays (TNTA), (b) 0.04 M of CuO-TNTA, (c) 0.05 M of CuO-TNTA, and (d) 0.06 M of CuO-TNTA.

As an illustration, the crystallite size of TNTA can be calculated using Debye Scherrer's Eq. (13) as follows (Fatimah *et al.*, 2022):

$$D = \frac{K.\lambda}{\beta cos\theta} \qquad (13)$$

with D = crystal size (nm), K = Scherrer constant = 0.9, λ = wavelength of X-ray radiation used = 0.15406 nm, β = Full Width at half maximum (FWHM) = 0.286 (should be converted to radian), and θ = the peak position of the TNTA in XRD pattern = (25.52/2) (should be converted to radian). From this formula, the crystallite size for TNTA is 28.5 nm as shown in **Table 3**.

Figure 5 represents the UV-Vis absorption spectra of different photocatalyst samples. The bandgap is evaluated by the Kubelka–Munk equation (Elysabeth *et al.*, 2021) and is presented in **Table 4**.

DOI: http://dx.doi.org/10.xxxxx/ijost.vXiX
p- ISSN 2528-1410 e- ISSN 2527-8045

The results indicate that all samples exhibit enhancement in terms of photo-response, as the onsets shift to the visible light region (> 400 nm) while the addition of CuO imposes bandgap values of 3.03, 2.98, and 2.96 eV, lower than the 3.16 eV recorded for the pure TiO_2 nanotube. The redshift can be reasoned by the presence of the CuO in TiO_2 nanotubes, possessing a bandgap of 1.2 eV (Sun *et al*., 2013). The red shift is more apparent in the case of CuO-TNTA with higher content of CuO while the lower content of CuO does not affect the optical properties significantly.

The UV-Vis Diffuse Reflectance Spectroscopy (DRS) method is based on measuring the UV-Vis intensity reflected by the sample. When the light (ultraviolet and/or visible) is irradiated by the material, some of it is absorbed, reflected, and transmitted in the form of spectra. The absorption of light causes the excitation of electrons from the ground to an excited state (Pratiwi and Nandiyanto, 2022). Using the Kubelka-Munk function F(R) and Tauc plot, the band gap energy (Eg) of the photocatalyst can be determined by Eq. (14) as follows:

$$[F(R)hv]^{1/2} = K\,(hv - Eg) \qquad (14)$$

with F(R) = $(1\text{-}R)^2/2R$, R = reflectance, *hv* = photon energy, and K = constant characteristic of TiO_2. For TNTA, a plot of $[F(R)\ hv]^{1/2}$ vs. *hv* must show a linear region just above the optical absorption edge (Ratnawati, 2014). The band gap energy can be found with the extrapolation of the linear portion of a Tauc plot to the hv axis, and the result is depicted in **Table 4**.

Table 3. The crystal size of various nanocomposites.

Nanocomposites	Anatase crystal size (nm)
TNTA (crystal)	28.5
0.04 M of CuO-TNTA	27.8
0.05 M of CuO-TNTA	27.0
0.06 M of CuO-TNTA	26.9

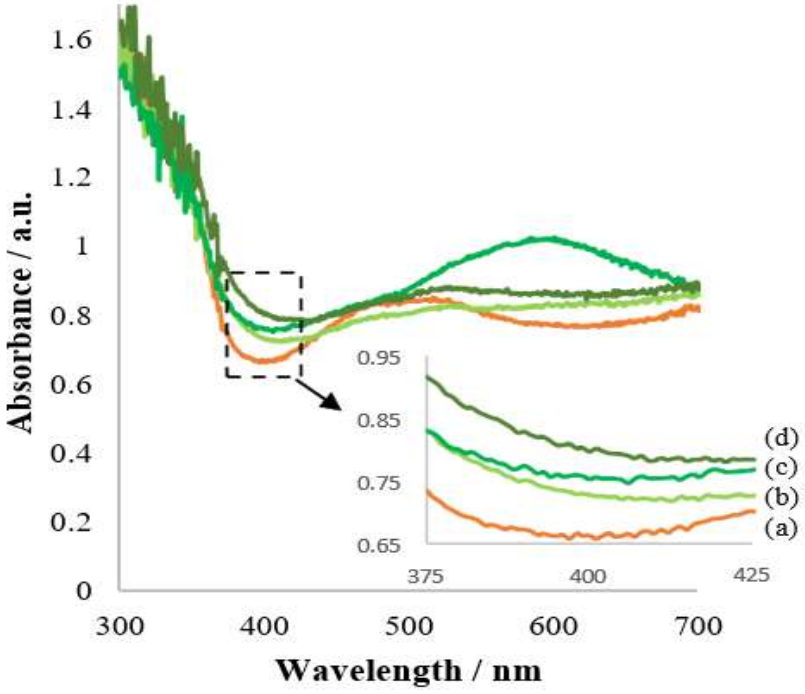

Figure 5. The UV-Vis DRS absorbance of different photocatalyst samples (a) TiO_2 nanotube arrays (TNTA), (b) 0.04 M of CuO-TNTA, (c) 0.05 M of CuO-TNTA, and (d) 0.06 M of CuO-TNTA.

DOI: http://dx.doi.org/10.xxxxx/ijost.vXiX
p- ISSN 2528-1410 e- ISSN 2527-8045

Table 4. Band-gap energy of various nanocomposites.

Types of Nanocomposites	Band-Gap Energy (eV)	Wavelength (nm)
TNTA	3.16	392
0.04 M of CuO-TNTA	3.03	409
0.05 M of CuO-TNTA	2.98	416
0.06 M of CuO-TNTA	2.96	419

4.2. Photocatalytic Test on Tartrazine Decolorization

Figure 6A depicts the photodegradation of tartrazine for two different pH values, in which it is evident that the photo-induced decolorization favors high pH. The adsorption-desorption properties on the surface of the catalysts are significantly affected by pH. This was related to the fact that the TiO_2 photocatalyst was negatively charged in the alkaline conditions due to the reaction between hydroxyl ions (OH^-) and h^+ to form hydroxyl radicals (OH•), which subsequently attack tartrazine, as also reported by previous researchers (Gupta *et al*., 2011).

Under acidic conditions, the number of hydroxyl ions is small, so the formation of hydroxyl radicals is limited. As a result, under acidic conditions, the reaction rate of the photocatalytic process is relatively slow. The photodegradation of tartrazine at pH = 11 for different photocatalyst samples is presented in **Figure 6B**.

The photo-induced decolorization of tartrazine is positively correlated with the amount of CuO present in CuO-TNTA composites. The highest rate of decolorization was obtained by the use of CuO-TNTA prepared with 0.06 M of Cu precursor, offering 64% degradation of tartrazine over 12 h illumination. In this case, CuO plays an important role in terms of inhibiting charge recombination, thereby facilitating faster separation and transfer of electrons and holes (Anantha Singh, & Ramesh, 2013).

Considering the band alignment between TiO_2 and CuO, we believe that the photoexcited electrons generated in the conduction band of TiO_2 are thermodynamically feasible to move to the more positive conduction band of CuO. Conversely, the holes generated in the valence band of CuO are transferred to the more negative valence band of TiO_2. The relatively low rate of photocatalytic reaction is most likely due to the limited surface area of the photocatalyst films (ca. 20 cm^2).

To calculate the photodegradation rate of tartrazine at various dopant CuO concentrations (**Figure 6B**), Eq. (12) was applied, and the results are depicted in **Table 5**.

The high value of the correlation coefficient (R^2) indicates that statistically, the first-order kinetic model is following the experimental data. The greater the value of k_1, the faster the photodegradation rate which results in high removal efficiency. This condition was achieved by a photocatalytic process using 0.06 M of CuO-TNTA.

DOI: http://dx.doi.org/10.xxxxx/ijost.vXiX
p- ISSN 2528-1410 e- ISSN 2527-8045

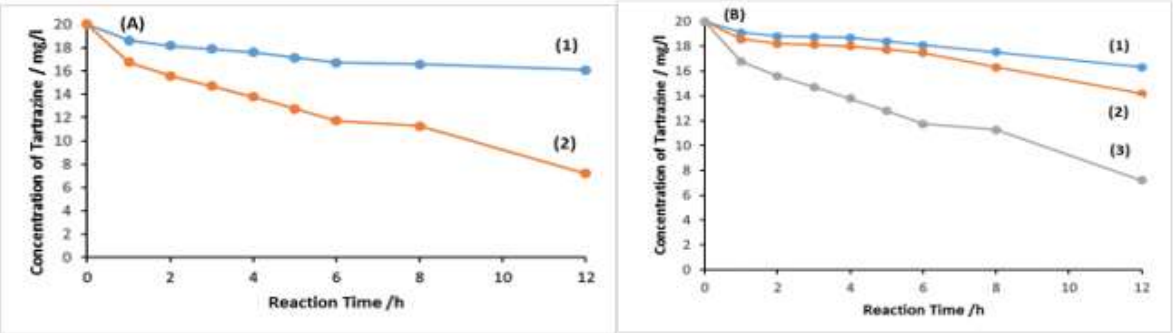

Figure 6. Photodegradation of tartrazine with 0.06 M CuO-TNTA at different pH (A) with pH = 4 (1), pH = 11 (2), and several photocatalysts (B) with TNTA (1), 0.04 M CuO-TNTA (2), 0.06 M CuO-TNTA (3) at pH = 11.

Table 5. Comparison of kinetic constants, k for the first-order reaction of tartrazine removal at various photocatalyst.

Photocatalysts	first-order pseudo model	
	k_1 (hours^{-1})	R^2
TNTA	0.0172	0.929
0.04M CuO-TNTA	0.0272	0.924
0.06M CuO-TNTA	0.0849	0.955

4.3. Electrocoagulation Test of the Tartrazine Decolorization and H_2 Production

The decolorization of tartrazine through electrocoagulation was conducted in a reactor with an Al plate as the anode and SS 316 plate as the cathode. **Figure 7A** shows the decolorization of tartrazine at different voltages of electrocoagulation, offering tartrazine removal of 56, 71, 82, and 88% at 20, 30, 40, and 50 V, respectively.

The positive correlation between the voltage and the removal rate of the redox target is unsurprising, as the reaction rate is directly proportional to the current, and the current is positively correlated to the electrical driving force, which was also reported by other authors (Syaichurrozi *et al.*, 2021).

At higher voltage, more electrons are extracted from the anode to produce Al^{3+} from Al, which, subsequently forms $Al(OH)_3$ serving as a coagulant. Furthermore, more electrons are transferred to the inert cathode to produce H_2 from the reduction of H_2O or protons.

Figure 7B displays the production of H_2 throughout 4 h operation, running at different voltages. It was found that the amount of H_2 generated from the processes is 1.52, 3.58, 10.86, and 17.03 mmol H_2 at 20, 30, 40, and 50 V, respectively. These results confirm the feasibility of the simultaneous removal of dye and production of fuel through the scheme proposed in this study. This result is following the findings that have been reported by previous researchers (Boroski *et al.*, 2009; Ates *et al.*, 2017; Syaichurrozi *et al.*, 2021).

To evaluate the tartrazine removal efficiency by electrocoagulation process at various voltages, the removal rates were calculated according to Eq. (12), and the results are in **Table 6**. From **Table 6**, it can be concluded that the higher the voltage, the greater the value of k_1, and therefore the rate of tartrazine removal is also faster.

DOI: http://dx.doi.org/10.xxxxx/ijost.vXiX
p- ISSN 2528-1410 e- ISSN 2527-8045

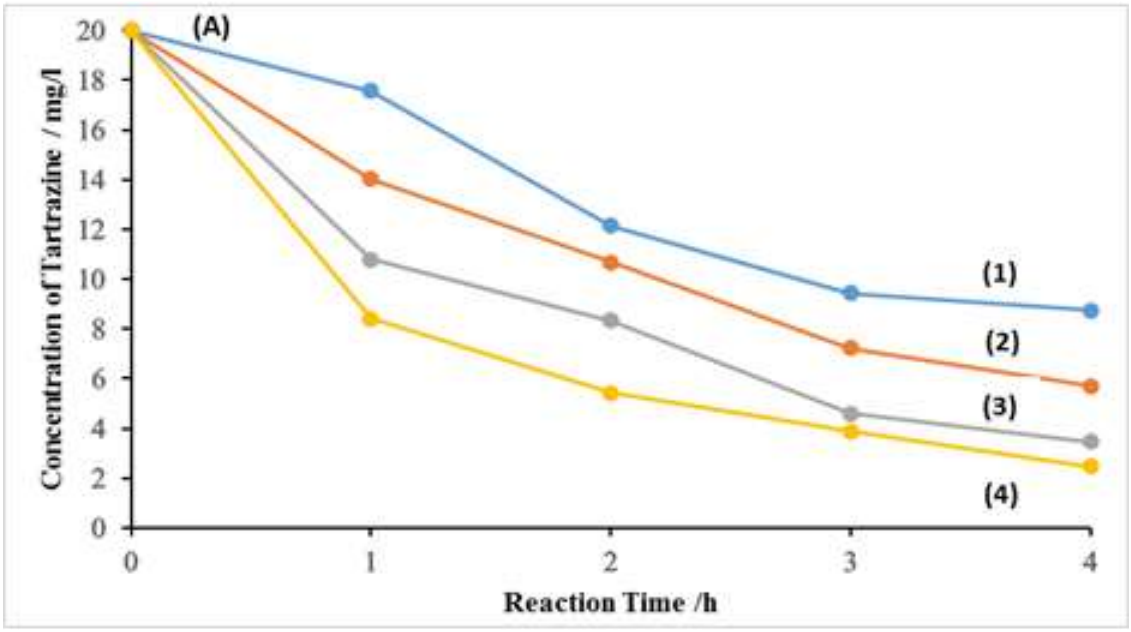

Figure 7. Degradation of tartrazine (A) H_2 production by electrocoagulation (B) as a function of time and at various voltages of 20 V (1), 30 V (2), 40 V (3), and 50 V (4) at pH = 11.

Figure 8A and **8B** respectively show the simultaneous decolorization of tartrazine and generation of H_2 in different modes of operation, namely photocatalysis, electrocoagulation, and the combination of both. In terms of tartrazine removal, 60% removal was obtained in the case of electrocoagulation only and 31% in the case of photocatalysis only. Upon combining both processes, 80% removal of tartrazine is achieved throughout 4 h. Similarly, in terms of H_2 production, the combination of electrocoagulation and photocatalysis staggeringly generates 1.84 mmol of H_2, much superior to those obtained by the operation of electrocoagulation (0.99 mmol) and photocatalysis (0.08 mmol). Since the electrocoagulation-photocatalysis

Combination managed to nearly double the total production of H_2 of the individual processes, the synergetic effect of both processes is plausible. It is likely that, in the case of the combined process, OH^- reacts not only with Al^{3+} but also with photo-excited

DOI: http://dx.doi.org/10.xxxxx/ijost.vXiX
p- ISSN 2528-1410 e- ISSN 2527-8045

holes to generate hydroxyl radicals. Combined with the electron-trapping role performed by CuO in CuO-TNTA composite, this scheme allows suppression of electron-hole recombination (Zangeneh *et al*., 2020).

Figure 9 represents the same comparative study of different operation modes for the decolorization of tartrazine, operating at a higher voltage (50 V), which further corroborates the effectiveness of the combined process, and the removal rates are presented in **Table 7**. The combination of photocatalysis and electrocoagulation processes has the highest rate constant for decreasing tartrazine concentration (**Table 7**). This means that this process combination provides the highest efficiency compared to other processes. This finding agreed with the results previously reported (Muttaqin *et al*., 2022) when they used different types of waste.

Table 6. The adsorption rate constant of tartrazine at various voltages.

Electrocoagulation	first-order pseudo model	
Voltage	k_1 (hours^{-1})	R^2
20 V	0.3275	0.908
30 V	0.3096	0.991
40 V	0.5041	0.970
50 V	0.5595	0.942

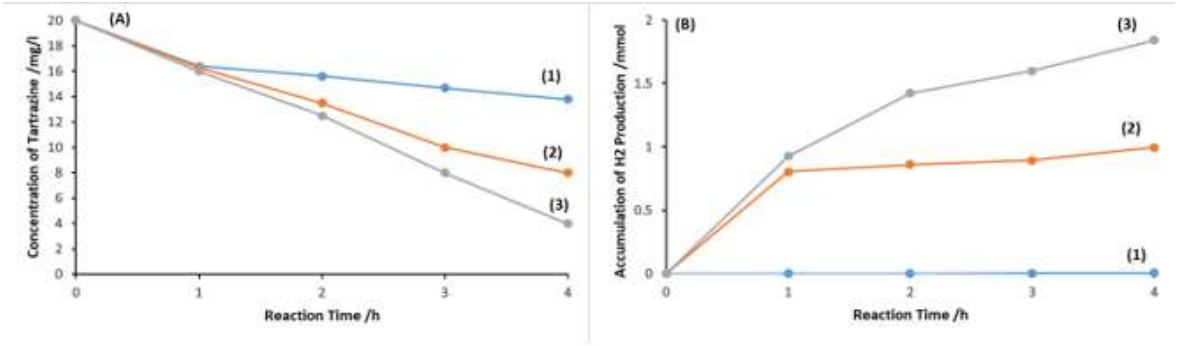

Figure 8. Degradation of tartrazine (A) and production of H_2 (B) at pH = 11, 20V as the function of time at different processes including (1) photocatalytic with CuO 0.06 M-TNTA, (2) electrocoagulation, and (3) combination of electrocoagulation–photocatalytic.

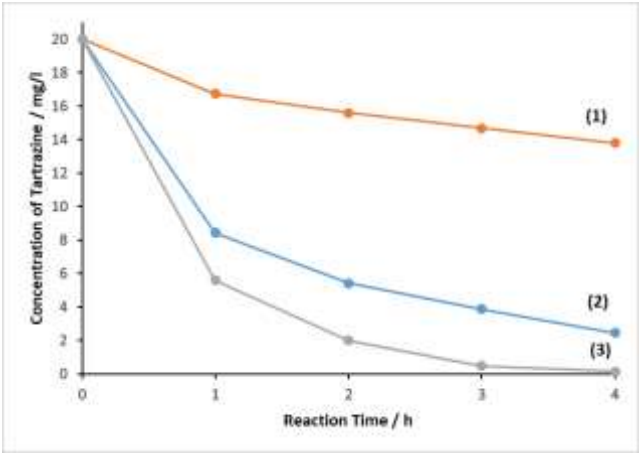

Figure 9. Degradation of tartrazine at pH = 11, 50 V as a function of time at (1) photocatalytic process with CuO 0.06 M-TNTA, (2) electrocoagulation, and (3) combination of electrocoagulation–photocatalytic.

DOI: http://dx.doi.org/10.xxxxx/ijost.vXiX
p- ISSN 2528-1410 e- ISSN 2527-8045

Table 7. The comparative value of the rate constant at different operation modes for the decolorization of tartrazine.

Treatment Process	first-order pseudo model	
	k_1 (hours^{-1})	R^2
Photocatalytic (P)	0.0272	0.924
Electrocoagulation (E)	0.5595	0.942
Combination of P and E	1.2022	0.998

Figure 10 shows the scheme of the combined processes of electrocoagulation and photocatalysis. In this scheme, tartrazine is degraded by the adsorption of $Al(OH)_3$ in the electrocoagulation process and it oxidizes by •OH or $•O^{2-}$ radicals in the photocatalytic process simultaneously. At the same time, H_2 produces by the reduction of H^+ in the cathode and on the photocatalyst surface. The glass sheath protects the cathode of SS 316 and CuO-TNTA photocatalyst plates to provide H_2 is collected and thereby the measurement becomes more accurate. In this combination process integrated into one reactor, operating conditions affect the efficiency of the waste treatment and H_2 production namely pH (Ates *et al.*, 2017), Voltage (Boroski *et al.*, 2009; Ates *et al.*, 2017; Syaichurrozi *et al.*, 2021), electrode materials, distance of the electrodes (Amri *et al.*, 2020), amount of the photocatalyst, the crystallite size, the concentration of waste (Nandiyanto *et al.*, 2016, Muttaqin *et al.*, 2022), and type of wastes (Safran *et al.*, 2018; Dindas *et al.*, 2020).

5. CONCLUSION

This study reports the combination of electrocoagulation and photocatalysis to simultaneously eliminate tartrazine dye and produce hydrogen in an integrated reactor. The deposition of CuO on TNTA photocatalyst using the SILAR method was successfully conducted, as confirmed by EDX analysis, TEM imaging, and SAED analysis. Upon the addition of CuO on TNTA, the redshift of the optical onset and bandgap lowering was also observed. The CuO-TNTA composite improves the photocatalytic activity of TiO_2. The combination of electrocoagulation and photocatalysis in eliminating tartrazine as well as producing H_2 is superior to each process, resulting in 80% tartrazine removal and 1.84 mmol H_2 productions. The significant improvement observed in this study suggests a synergetic effect between both processes. The results reported in this study are expected to pave the way to an integrated system capable of effectively removing pollutants, while, at the same time, producing H_2 as a green fuel.

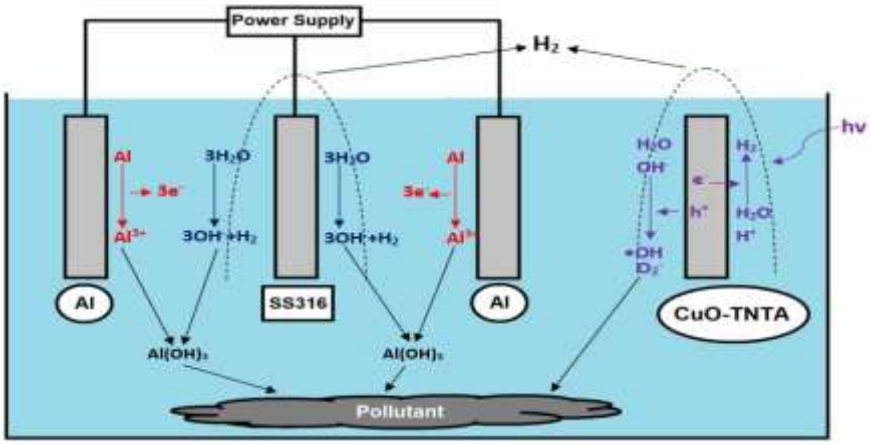

Figure 10. The mechanisms used in the combination of electrocoagulation and photocatalytic process.

DOI: http://dx.doi.org/10.xxxxx/ijost.vXiX
p- ISSN 2528-1410 e- ISSN 2527-8045

6. ACKNOWLEDGMENT

The authors appreciate the DRPM Universitas Indonesia for the financial support provided for this research through the Program Hibah PUTI Q2 Universitas Indonesia and the Contract Number: NKB-1743/UN2.RST/HKP.05.00/2020.

7. AUTHORS' NOTE

The authors declare that there is no conflict of interest regarding the publication of this article. The authors confirmed that the paper was free of plagiarism.

8. REFERENCES

Ahn, K., Kim, K., and Kim, J. (2015). Thermal conductivity and electric properties of epoxy composites filled with TiO_2-coated copper nanowire. *Polymer*, *76*, 313-320.

Amin, K. A., and Al-Shehri F. S. (2018). Toxicological and safety assessment of tartrazine as a synthetic food additive on health biomarkers: A review. *African Journal of Biotechnology*, *17*(6), 139-149.

Amri, N., Abdullah, A. Z., and Ismail, S. (2020). Removal efficiency of acid red 18 dye from aqueous solution using different aluminium-based electrode materials by electrocoagulation process. *Indonesian Journal of Chemistry, 20*(3), 536 – 544.

Anantha Singh, T. S., and Ramesh, S. T. (2013). New trends in electrocoagulation for the removal of dyes from wastewater: a review. *Environmental Engineering Science*, *30*(7), 333-349.

Aoudjit L, Ziou D, Touahra F., and Mahidine, S. (2021). Photocatalytic degradation of tartrazine dyes using tio_2–chitosan beads under sun light irradiation. *Russian Journal Physic Chemistry A*, *95*(5), 1069–1076.

Ates, H., Dizge, N., and Yatmaz, H. C. (2017). Combined process of electrocoagulation and photocatalytic degradation for the treatment of olive washing wastewater. *Water Science and Technology, 75*(1), 141-154.

Boroski, M., Rodrigues, A. C., Garcia, J. C., Sampaio, L. C., Nozaki, J., and Hioka, N. (2009). Combined electrocoagulation and TiO_2 photoassisted treatment applied to wastewater effluents from pharmaceutical and cosmetic industries. *Journal of Hazardous Materials*, *162*(1), 448-454.

Byoud, F., Wakrim, A., Benhsinat, C., and Zaina, Z. (2017). Electrocoagulation treatment of the food dye waste industry: Theoretical and experimental study. *Journal of Materials and Environmental Science*, *8*(2), 4301-4312.

Cao, D., Wang, Q., Wu, Y., Zhu, S., Jia, J., and Wang, R. (2020). Solvothermal synthesis and enhanced photocatalytic hydrogen production of Bi/Bi_2MoO_6 co-sensitized TiO_2 nanotube arrays. *Separation and Purification Technology*, *250*, 117132.

Dindaş, G. B., Çalışkan, Y., Celebi, E. E., Tekbaş, M., Bektaş, N., and Yatmaz, H. C. (2020). Treatment of pharmaceutical wastewater by combination of electrocoagulation, electro-fenton and photocatalytic oxidation processes. *Journal of Environmental Chemical Engineering*, *8*(3), 103777.

Elangovan, M., Bharathaiyengar, S.M., and Ettiyappan, J. P. (2021). Photocatalytic degradation of diclofenac using TiO2- CdS heterojunction catalysts under visible light irradiation. *Environmental Science and Pollution Research*, *28*, 18186-18200.

Elysabeth, T., Mulia, K., and Ibadurrohman, M., (2021). A comparative study of CuO deposition methods on titania nanotube arrays for photoelectrocatalytic ammonia degradation and hydrogen production. *International Journal of Hydrogen Energy*, *46*(53), 26873-26885.

Fatimah, S., Ragadhita, R., Al Husaeni, D. F., and Nandiyanto, A. B. D. (2022). How to calculate crystallite size from x-ray diffraction (XRD) using Scherrer method. *ASEAN Journal of Science and Engineering*, *2*(1), 65-76.

Gupta, V. K., Jain, R., Nayak A., Agarwal, S., and Shrivastavac, M. (2011). Removal of the hazardous dye-tartrazine by photodegradation on titanium dioxide surface. *Material Science and Engineering: C*, *31*(5), 1062-1067.

Hashim, K. S., Al-Khaddar, R., Shaw, A., Kot, P., Al-Jumeily, D., Alwash, R., and Aljefery, M. H. (2020). Electrocoagulation as an eco-friendly river water treatment method. *Advanced Water Research Engineering and Management*, *39*, 219–235.

Janczarek, M., and Kowalska, E. (2017). On the origin of enhanced photocatalytic activity of copper-modified titania in the oxidative reaction systems. *Catalysts*, *7*(11), 317.

Javaid, R., and Qazi, U. Y. (2019). Catalytic oxidation process for the degradation of synthetic dyes: An overview. *International Journal Environmental Research and Public Health*, *16*(11), 2-27.

Jia, Y., Liu, P., Wang, Q., Wu, Y., Cao, D., and Qiao, Q. A. (2021). Construction of Bi2S3-BiOBr nanosheets on TiO2 NTA as the effective photocatalysts: Pollutant removal, photoelectric conversion, and hydrogen generation. *Journal of Colloid and Interface Science*, *585*, 459-469.

Kartikowati, C. W., Arif, A. F., Arutanti, O., and Ogi, T. (2021) Carbon-coated Single-phase Ti4O7 Nanoparticles as Electrocatalyst Support. *Indonesian Journal of Science and Technology*, *6*(1), 235-242.

Meng, A., Zhang, J., Xu, D., Cheng, B., and Yu, J. (2016). Enhanced photocatalytic H2-production activity of anatase TiO2 nanosheet by selectively depositing dual-cocatalysts on {101} and {001} facets. *Applied Catalysis B: Environmental*, *198*, 286-294.

Momeni, M. M. (2015). Fabrication of copper decorated tungsten oxide–titanium oxide nanotubes by photochemical deposition technique and their photocatalytic application under visible light. *Applied Surface Science*, *357*, 160-166.

Muttaqin, R., Pratiwi, R., Ratnawati, Dewi, E. L., Ibadurrohman, M., and Slamet. (2022). Degradation of methylene blue-ciprofloxacin and hydrogen production simultaneously using combination of electrocoagulation and photocatalytic process with Fe-TiNTAs. *International Journal of Hydrogen Energy*, *47*(14), 18272-18284.

Nandiyanto, A. B. D., Sofiani, D., Permatasari, N., Sucahya, T. N., Wiryani, A. S., Purnamasari, A., Rusli, A., and Prima, E. C. (2016). Photodecomposition profile of organic material during the partial solar eclipse of 9 March 2016 and its correlation with organic material

DOI: http://dx.doi.org/10.xxxxx/ijost.vXiX
p- ISSN 2528-1410 e- ISSN 2527-8045

concentration and photocatalyst amount. *Indonesian Journal of Science and Technology*, *1*(2), 132-155.

Nandiyanto, A.B.D., Ragadhita, R., Oktiani, R., Sukmafitri, A., and Fiandini, M. (2020). Crystallite sizes on the photocatalytic performance of submicron WO_3 particles. *Journal of Engineering Science and Technology*, *15*(3), 1506-1519.

Okoniewska, E. (2021). Removal of selected dyes on activated carbons. *Sustainability*, *13*(8), 4300.

Pelawi, L. F., Slamet, and Elysabeth, T. (2019). Combination of electrocoagulation and photocatalysis for hydrogen production and decolorization of tartrazine dyes using CuO-TiO_2 nanotubes photocatalysts. *AIP Conference Proceeding*, *2223*, 040001-1–040001-8.

Popli, S., and Patel, U. D. (2015). Destruction of azo dyes by anaerobic-aerobic sequential biological treatment: A review. *International Journal of Environmental Science and Technology*, *12*(1), 405–420.

Pourgholi, M., Masoomi Jahandizi, R., Miranzadeh, M., Beigi, O. H., and Dehghan, S. (2018). Removal of Dye and COD from textile wastewater using AOP (UV/O3, UV/H2O2, O3/H2O2 and UV/H2O2/O3). *Journal of Environmental Health and Sustainable Development*, *3*(4), 630-636.

Pratiwi, R. A., and Nandiyanto, A. B. D. (2021). How to read and interpret UV-VIS spectrophotometric results in determining the structure of chemical compounds. *Indonesian Journal of Educational Research and Technology*, *2*(1), 1-20.

Ratnawati, Gunlazuardi, J., and Slamet. (2015). Development of titania nanotube arrays: The roles of water content and annealing atmosphere. *Materials Chemistry and Physics*, *160*, 111-118.

Ratnawati, Gunlazuardi, J., Dewi E.L., and Slamet. (2014). Effect of NaBF4 addition on the anodic synthesis of TiO2 nanotube arrays photocatalyst for production of hydrogen from glycerol–water solution. *International Journal of Hydrogen Energy*, *39*(30), 16927-16935.

Raul, P. K., Senapati, S., Sahoo, A. K., Umlong, I. M., Devi, R. R., Thakur, A. J., and Veer, V. (2014). CuO nanorods: a potential and efficient adsorbent in water purification. *Rsc Advances*, *4*(76), 40580-40587.

Russo, A. V., Merlo, B. G., and Jacobo, S. E. (2021). Adsorption and catalytic degradation of Tartrazine in aqueous medium by a Fe-modified zeolite. *Cleaner Engineering and Technology*, *4*, 100211.

Sang, L., Zhang, S., Zhang, J., Yu, Z., Bai, G., and Du, C. (2019). TiO2 nanotube arrays decorated with plasmonic Cu, CuO nanoparticles, and eosin Y dye as efficient photoanode for water splitting. *Materials Chemistry and Physics*, *231*, 27-32.

Santos, L. M., Amorim, K. P. D., Andrade, L. S., Batista, P. S., Trovó, A. G., and Machado, A. E. (2015). Dye degradation enhanced by coupling electrochemical process and heterogeneous photocatalysis. *Journal of the Brazilian Chemical Society*, *26*, 1817-1823.

Scott, R., Mudimbi, P., Miller, M. E., Magnuson, M., Willison, S., Phillips, R., and Harper Jr, W. F. (2017). Advanced oxidation of tartrazine and brilliant blue with pulsed ultraviolet light emitting diodes. *Water Environment Research*, *89*(1), 24-31.

DOI: http://dx.doi.org/10.xxxxx/ijost.vXiX
p- ISSN 2528-1410 e- ISSN 2527-8045

Sharfan, N., Shobri, A., Anindria, F. A., Mauricio, R., Tafsili, M. A. B., and Slamet, S. (2018). Treatment of batik industry waste with a combination of electrocoagulation and photocatalysis. *Chemical Engineering*, *9*(5), 936-943.

Slamet, and Kurniawan, R. (2018). Degradation of tartrazine and hydrogen production simultaneously with combination of photocatalysis-electrocoagulation. *AIP Conferenvce Proceeding*, *2024*, 020064-1–020064-9.

Slamet, Ratnawati, Gunlazuardi, J., and Dewi, E. L. (2017). Enhanced photocatalytic activity of Pt deposited on titania nanotube arrays for the hydrogen production with glycerol as a sacrificial agent. *International Journal of Hydrogen Energy*, *42*(38), 24014-24025.

Soufi, A., Hajjaoui, H., Elmoubarki, R., Abdennouri, M., Qourzal, S., and Barka, N. (2022). Heterogeneous Fenton-like degradation of tartrazine using CuFe2O4 nanoparticles synthesized by sol-gel combustion. *Applied Surface Science Advances*, *9*, 100251.

Sun, Q., Li, Y., Sun, X., and Dong, L. (2013). Improved photoelectrical performance of single-crystal TiO_2 nanorod arrays by surface sensitization with copper quantum dots. *ACS Sustainable Chemical Engineering, 1*, 798-804.

Syaichurrozi, I., Sarto, S., Sediawan, W. B., and Hidayat, M. (2021). Effect of current and initial pH on electrocoagulation in treating the distillery spent wash with very high pollutant content. *Water, 13*(11), 1-20.

Vaiano, V., Iervolino, G., and Sannino, D. (2016). Photocatalytic removal of tartrazine dye from aqueous samples on LaFeO 3/ZnO photocatalysts. *Chemical Engineering Transactions*, *52*, 847-852.

Yolanda, Y. D., and Nandiyanto, A. B. D. (2022). How to read and calculate diameter size from electron microscopy images. *ASEAN Journal of Science and Engineering Education*, *2*(1), 11-36.

Zangeneh, H., Farhadian, M., and Zinatizadeh, A. A. (2020). N (Urea) and CN (L-Asparagine) doped TiO2-CuO nanocomposites: fabrication, characterization and photodegradation of direct red 16. *Journal of Environmental Chemical Engineering*, *8*(1), 103639.

Zhu, S., Wang, Q., Cao, D., Zhao, S., Xu, W., Li, C., and Wang, Y. (2022). CdTe and Ag nanoparticles co-modified TiO2 nanotube arrays for the enhanced wastewater treatment and hydrogen production. *Journal of Environmental Chemical Engineering*, *10*(2), 107207.

DOI: http://dx.doi.org/10.xxxxx/ijost.vXiX
p- ISSN 2528-1410 e- ISSN 2527-8045